Supplementary Information

Ultrafast Dynamics of Self-hybridized Exciton-Polaritons in WSe_2

Niu Xu[1,2,3+], Jin Yang[1,2,3+], Kaizhen Liu[1,2,3+], Weiming Song[1,2,3], Binxiong Lu[1,2,3], Zhiying Li[1,2,3], Baowen Li[1,4,5], Jin-Hui Zhong[1,2,3]*

[1]State Key Laboratory of Quantum Functional Materials, Shenzhen Key Laboratory of Phononics and Intelligent Thermal Materials, Department of Materials Science and Engineering, Southern University of Science and Technology, Shenzhen 518055, China

[2]Guangdong Provincial Key Laboratory of Sustainable Biomimetic Materials and Green Energy, Southern University of Science and Technology, Shenzhen 518055, China

[3]Institute of Innovative Materials, Southern University of Science and Technology, Shenzhen 518055, China

[4]Department of Physics, Southern University of Science and Technology, Shenzhen 518005, China

[5]School of Microelectronics, Southern University of Science and Technology, Shenzhen 518005, China

[+]These authors contribute equally to this work.

*Email: zhongjh@sustech.edu.cn

Table of Contents

Section 1. FP cavity mode calculation and angle resolved spectra of the self-hybridized WSe_2.

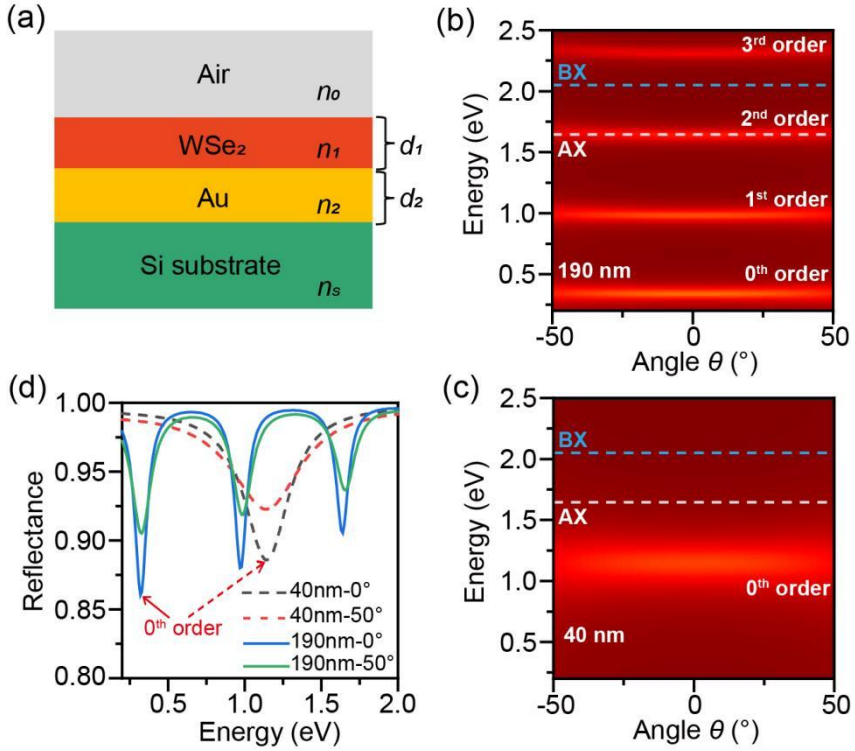

Supplementary Figure 1. FP cavity modes calculated using the transfer matrix method (TMM). (a) Schematic diagram of the sample structure, where n is the refractive index of the material and d represents the thickness of the layered material. (b,c) FP cavity modes in 190 nm (b) and 40 nm (c) thick layered material. The white and blue dashed lines indicate the energies of the A and B excitons, respectively. (d) Reflectance spectra of the cavity modes extracted from (b) and (c) at $\theta = 0^\circ$ and 50°.

The FP cavity modes in a layer with thicknesses of d = 190 nm and 40 nm, calculated based on the sample configuration in Supplementary Fig. 1a, are presented in Supplementary Fig. 1b and 2c, respectively. We use n = 4.6 without exciton resonance to mimic the responses of WSe_2. The FP cavity mode satisfies $2nd = (m + \frac{\varphi(\lambda)}{2\pi})\lambda$, where $\varphi(\lambda)$ is the total phase shift introduced by reflections at the upper and lower

interfaces.[1, 2] The 0th order mode arises because the sample thickness d_1 is much smaller than its resonant wavelength (d = 190 nm, $\lambda_{\text{zeroth order}}$ = 3875 nm; d = 40 nm, $\lambda_{\text{zeroth order}}$ = 1083 nm), making it a resonance determined primarily by the interfacial reflection phase shifts.[3, 4] As a result, this mode exhibits no dispersion, as shown in Supplementary Fig. 1d, where the resonance peak energies at $\theta = 0^\circ$ and 50° coincide. The phase shifts for the 0-order mode in the layer with thicknesses of 190 nm and 40 nm are 0.91π and 0.68π, respectively. For the 190 nm thick sample, the phase shifts of the first- to third-order modes are φ(1272 nm) = 0.75π, φ(757.5 nm) = 0.62π, and φ(535.6 nm) = 0.53π. The second order mode of 190 nm thick cavity is resonant with AX of WSe_2, ensuring an efficient exciton-cavity coupling. The energy difference between the cavity mode at 40 nm and the AX energy in WSe_2 is 500 meV, which is greater than the Rabi splitting value of 190 meV in the strong coupling system. Therefore, this cavity mode does not strongly couple with the AX.

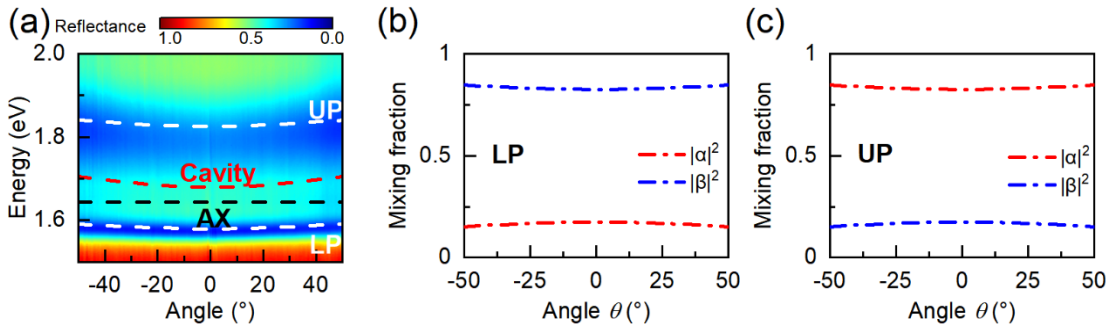

Supplementary Figure 2. Angle-resolved reflectance spectra of the 170 nm thick WSe_2 flake. (a) Color maps of experimentally measured angle-resolved reflectance spectra. The calculated UP, LP, cavity mode and uncoupled AX energy positions are presented by dashed lines. (b-c) Fractions of excitons (blue) and cavity photons (red) in LP (b) and UP (c) of the 170 nm thick flake as a function of incidence angle. Blue

detuning leads to a significant difference in the exciton-photon fractions between the UP and LP branches.

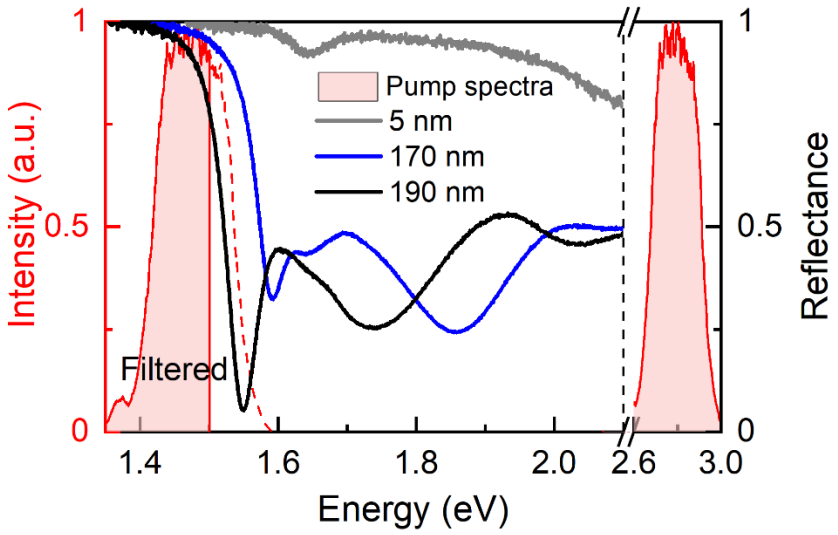

Supplementary Figure 3. Pump pulse spectra. Spectra of 1.47 eV (left) and 2.76 eV (right) pump light used in TR measurements (red shaded), and steady state reflection spectra of 5 nm, 170 nm, 190 nm thick WSe_2 flakes (lines) at $\theta = 30°$, respectively.

As shown in Supplementary Fig. 3, the 1.47 eV pump beam is filtered using an 825 nm (1.5 eV) long-pass filter to ensure that only the LP state is excited at an incident angle of 30°.

Section 2. TR spectra of thin WSe_2 flakes.

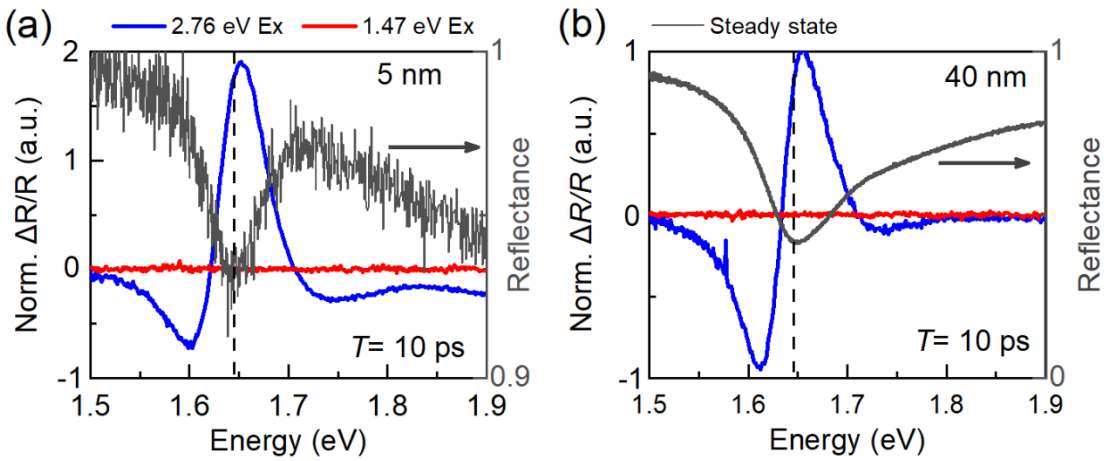

Supplementary Figure 4. Comparison of TR spectra with steady state reflectance spectra for 5 nm and 40 nm thick flakes. Steady state reflectance spectra (grey) and TR spectra at T = 10 ps of the 5 nm (a), and 40 nm (b) thick flakes under 1.47 eV (red) and 2.76 eV (blue) excitation. Amplitudes of TR signals are normalized by AX positive peaks intensity maxima.

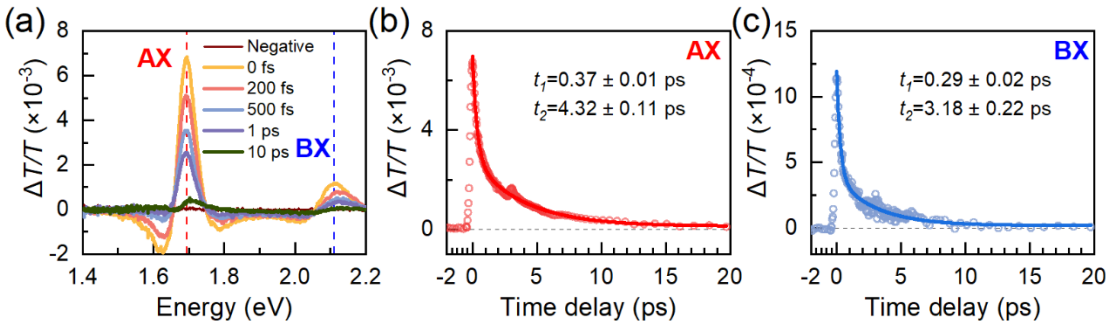

Supplementary Figure 5. Transient transmission spectra of monolayer WSe_2. (a) Representative transient transmission spectra at selected delay times of monolayer WSe_2 film under 2.76 eV excitation. Positive ground state bleaching (GSB) peak at the exciton energies and negative peaks resulting from excitation induced dephasing (EID) effect are observed. (b-c) Peak dynamics (circles) extracted from the positive peak maximum of AX response (b) at E = 1.7 eV, BX response (c) at E = 2.11 eV, and fitted curves (lines) using a bi-exponential function. The time constants are listed in the corresponding figure.

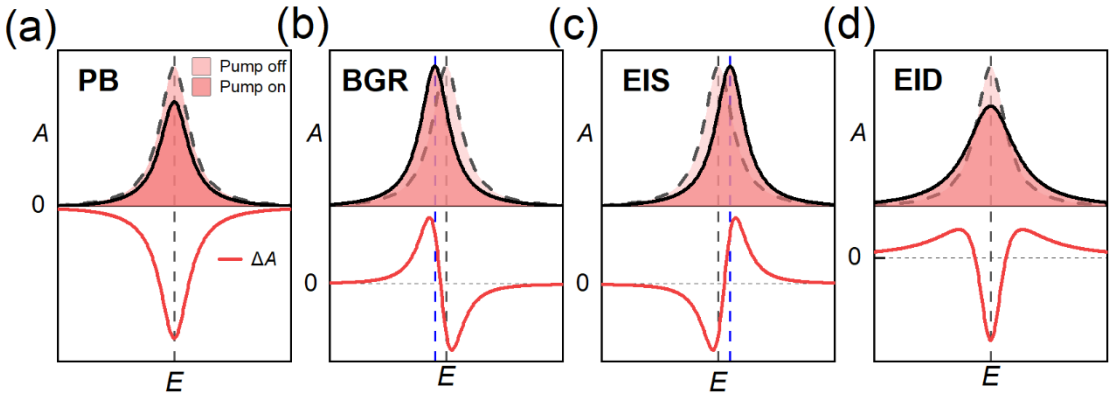

Supplementary Figure 6. Schematic diagrams of different nonlinearities for semiconductor excitons due to many-body interactions. (a) Pauli blocking (PB) reduces the transition dipole moment, exhibits a pure bleaching-type signal. (b) Bandgap renormalization (BGR) redshifts the transition state energy, resulting in a derivative line shape. (c) Excitation induced shifts (EIS) blueshifts the transition state energy, resulting in a derivative line shape which is out of phase with BGR line shape. (d) Excitation induced dephasing (EID) increases the damping rate of the optical transition, leading to a line shape broadening. The differential spectrum exhibits a negative peak in the center and positive side lobes on both sides.

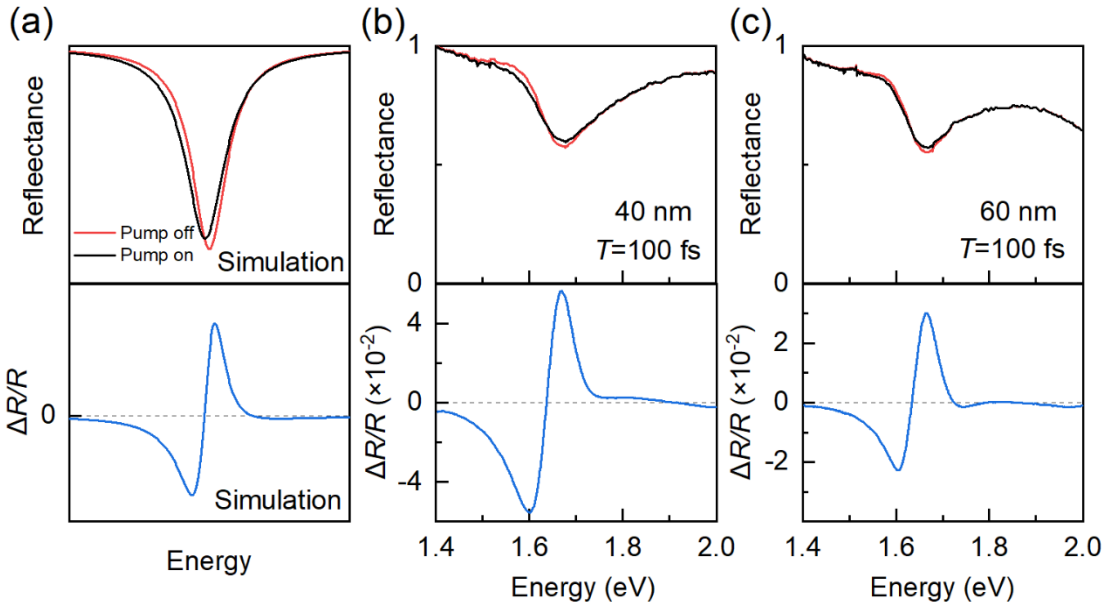

105

106 **Supplementary Figure 7. Schematic diagrams of the nonlinearities for thick WSe2**

107 **flakes.** (a) Simulated probe reflectance spectra in the presence and absence of pump

108 pulse (top) composed of Pauli blocking (PB), bandgap renormalization (BGR) and

109 excitation induced dephasing (EID) effects. These many-body interactions result in a

110 derivative line shape of the TR spectrum (bottom). (b-c) Experimental probe reflectance

111 spectra in the presence and absence of pump pulse (top) and the corresponding TR

112 spectra of 40 nm (b) and 60 nm (c) thick flakes at $T = 100$ fs.

113

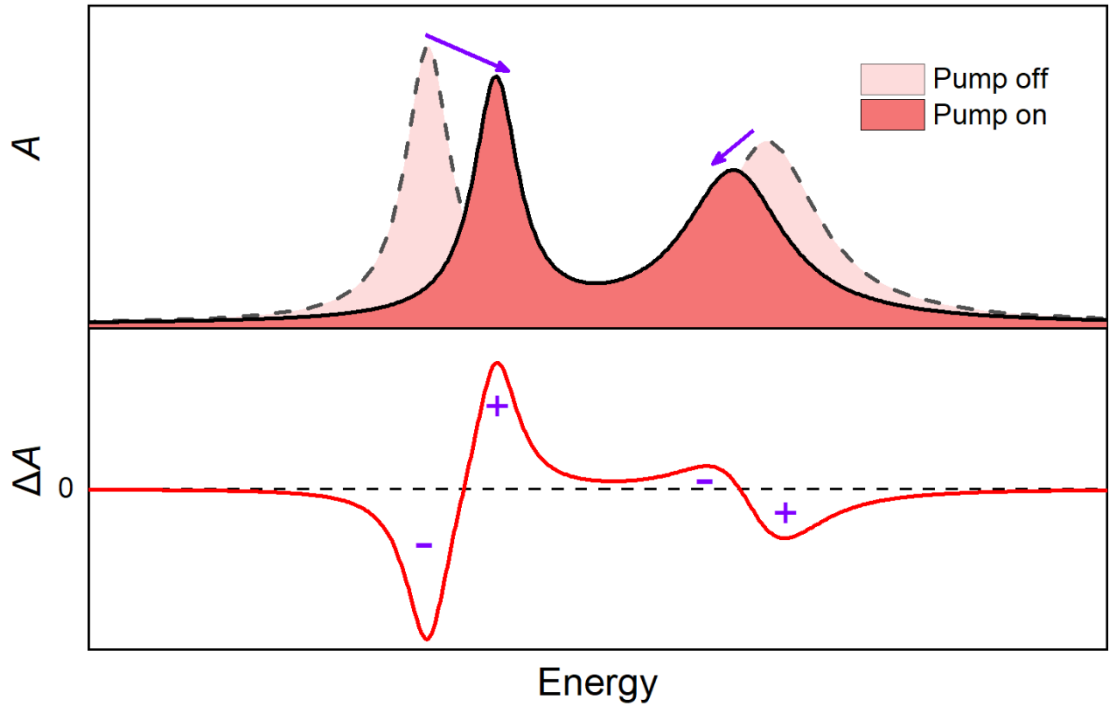

Supplementary Figure 8. Schematic diagrams of nonlinearities result from Rabi contraction. Rabi contraction reduces coupling strength due to the Pauli blocking effect and thus lead to redshift of UP and blueshift of LP.[5] In this case, the symmetries of LP and UP line shapes are opposite.

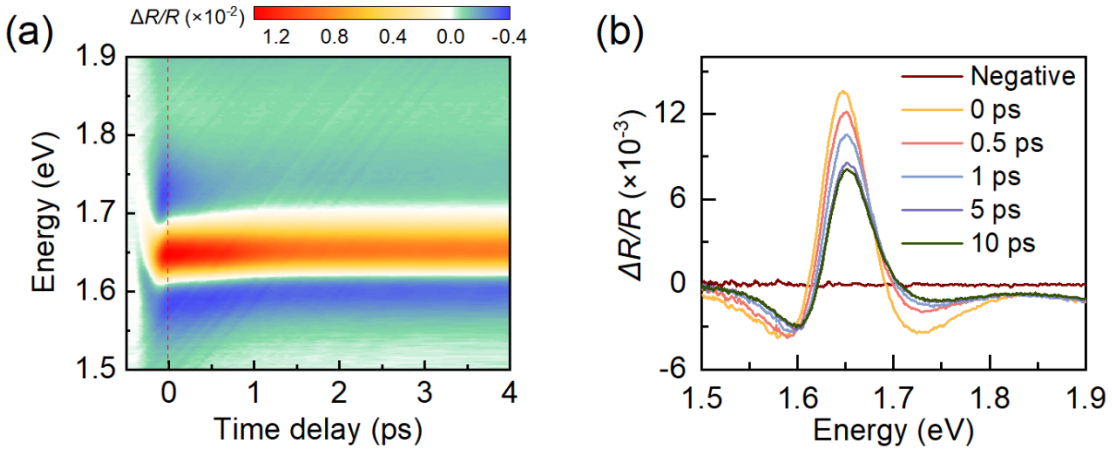

Supplementary Figure 9. Transient reflection (TR) spectra of the 5 nm thick WSe_2 flake. False-color map (a) and representative Δ*R*/*R* spectra at selected times (b) under 2.76 eV excitation. Strong initial EID induced broadening can be observed. With increasing time delay, the peak becomes narrowed because of the decreased EID effect.

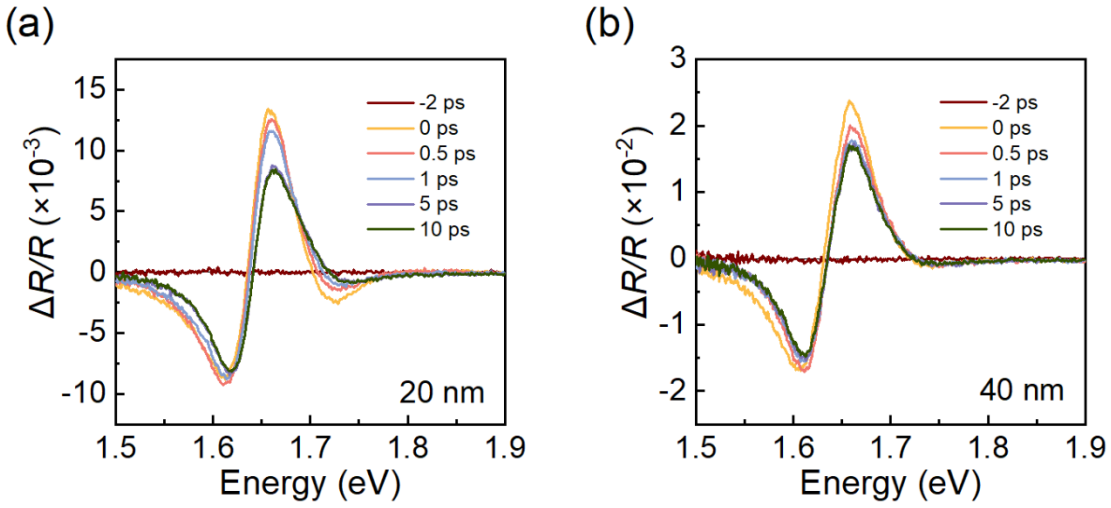

Supplementary Figure 10. TR spectra of the 20 nm and 40 nm thick WSe_2 flakes under 2.76 eV excitation, dominated by derivative line shapes.

As shown in Supplementary Fig. 10a, within the first few picoseconds, the AX positive peak of 20 nm thick flake is much stronger than the negative one. What's more, there is a weak negative peak at the high energy side, a feature that is seen for the 5 nm thick flake (Supplementary Fig. 4a) and the monolayer (Supplementary Fig. 5). However, the negative signal at 1.72 eV is much weaker compared to that at 1.62 eV, significantly different from the two thinner flakes. After 5 ps, the intensities of positive (1.67 eV) and negative (1.62 eV) peaks become comparable. As for 40 nm thick flake (Supplementary Fig. 10b), the negative signal at high energy side is hardly to be seen. Hence, we anticipate that for thicker flakes (170 and 190 nm), their TR spectra should also display derivative line shapes.

Section 3. Pump fluence-dependent TR spectra of WSe_2 flakes with different thicknesses.

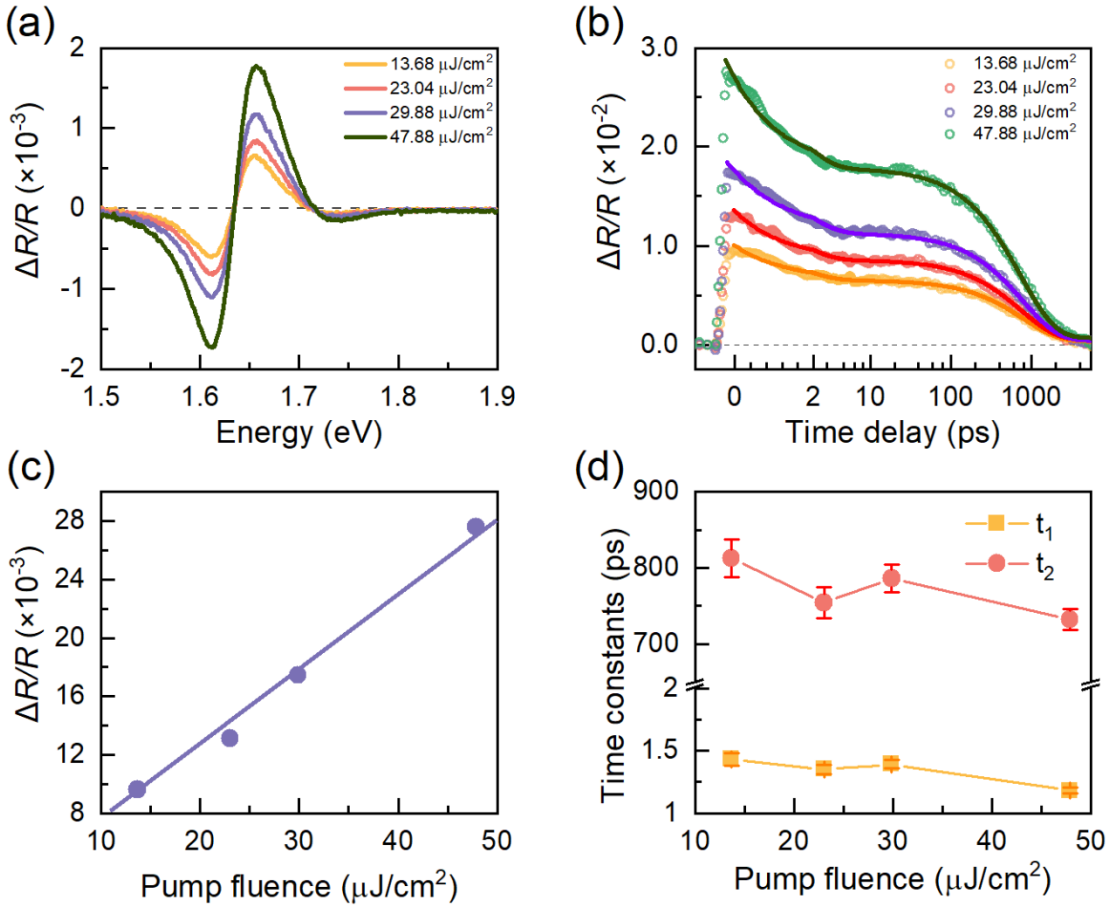

Supplementary Fig. 11. Pump fluence-dependent TR spectra of 40 nm thick WSe_2 flake under 2.76 eV excitation. (a) Representative $\Delta R/R$ spectra at T = 10 ps of the 40 nm thick WSe_2 flake under different pump fluences. (b) Peak dynamics (circles) extracted from the positive peak maximum of AX response at E = 1.67 eV under different pump fluences and fitted curves (lines) using a bi-exponential function. (c) Maximum intensity at T = 280 fs of the AX dynamics (symbols) fitted by a linear function (line), showing linear dependence with pump fluence. (d) Fitted time constants from the fitted curves in (b).

Supplementary Fig. 11a shows the TR spectra of the 40 nm thick WSe_2 flake under different pump fluences. AX peak dynamics taken at the positive maxima (E = 1.67 eV) are shown in Supplementary Fig. 11b (circles). The TR signal amplitude scales linearly with the pump fluence (Supplementary Fig. 11c). This ensures that strong nonlinear effects associated with high excitation densities, such as the Mott transition and multiphoton absorption, can be reasonably excluded. Bi-exponential fitting of the dynamics, shown as solid lines in Supplementary Fig. 11b, well reproduce the experimental data. The fitted parameters are listed in Supplementary Table 1 and plotted in Supplementary Fig. 11d. The first process (t_1~ 1.5 ps) can be assigned to the exciton formation process in TMD materials under above bandgap excitation, which also speeds up with increasing pump fluence. The second process (t_2) represents the interband recombination. Note that t_2 decreases with increasing pump fluence, indicating that the recombination is dominated by exciton-exciton annihilation (EEA). We further note that the recombination is significantly slower compared to that in atomically thin WSe_2 (~ 4 ps) because of the indirect bandgap nature of thick flakes (d = 40 nm).

Supplementary Table 1. Time constants of AX dynamics of 40 nm thick WSe_2 flake under 2.76 eV excitation fitted by bi-exponential function.

Pump fluence(μJ/cm^2)	t_1 (ps)	t_2 (ps)
13.68	1.43±0.05	812.65±25.10
23.04	1.35±0.04	753.91±20.09
29.88	1.39±0.033	786.28±17.96
47.88	1.18±0.026	732.06±13.51

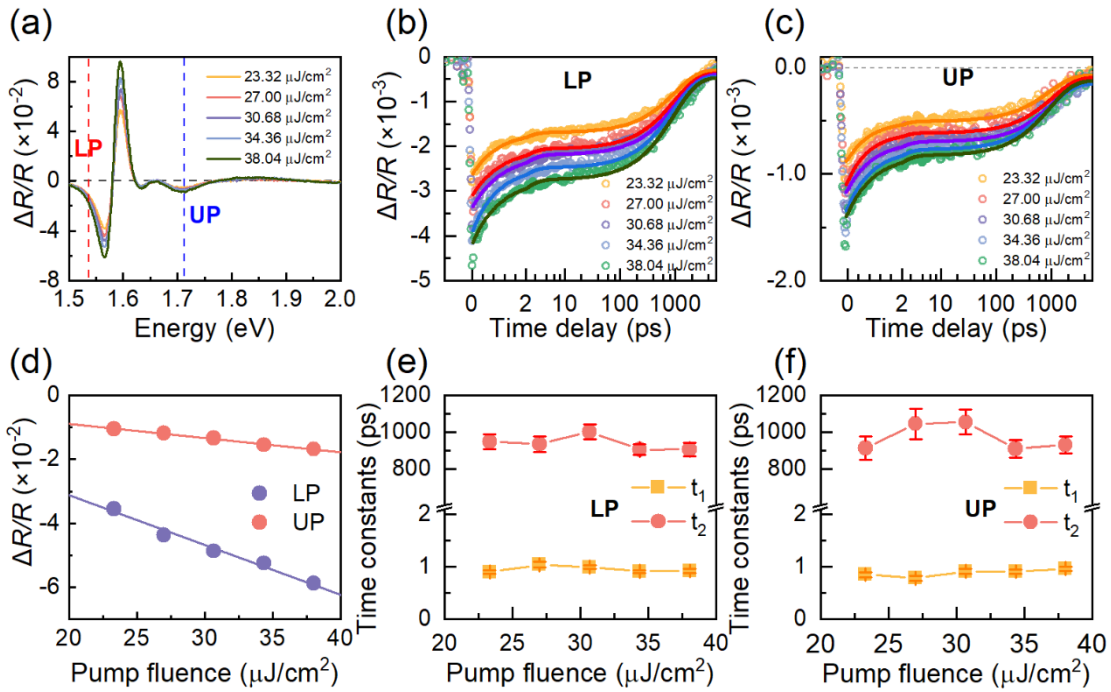

168

169 **Supplementary Figure 12. Pump fluence dependent TR spectra of the 170 nm**
170 **thick WSe_2 flake under 1.47 eV excitation.** (a) Representative $\Delta R/R$ spectra at $T = 10$
171 ps. (b-c) Experimental dynamics (cycles) and fitted lines by a bi-exponential function
172 of LP (b) and UP (c). (d) Minimum intensity at $T = 0$ fs of LP (violet) and UP (red)
173 dynamics fitted by a linear function (lines), showing linear dependence with pump
174 fluence. (e-f) Fitted time constants of LP (e) and UP (f) as a function of pump fluence.

175 We also studied pump fluence dependent polariton dynamics of the 170 nm thick WSe_2
176 flake under 1.47 eV excitation (Supplementary Fig. 12a) using bi-exponential fitting.
177 The signal amplitudes of both UP and LP show linear dependence with pump fluence
178 (Supplementary Fig. 12d), confirming that all experiments were carried out within the
179 linear response regime of the sample. LP and UP dynamics are fitted by bi-exponential
180 functions (Supplementary Fig. 12b-c). The fitted time parameters are listed in
181 Supplementary Table 2 and plotted in Supplementary Fig. 12e-f, showing negligible

dependence with pump fluence. This indicates that the relaxation of polaritons does not involve many-body interactions like polariton-polariton annihilation (PPA).

The results for the 190 nm thick flake are shown in Supplementary Fig. 13 and Supplementary Table 3, showing similar trends as that of the 170 nm thick flake.

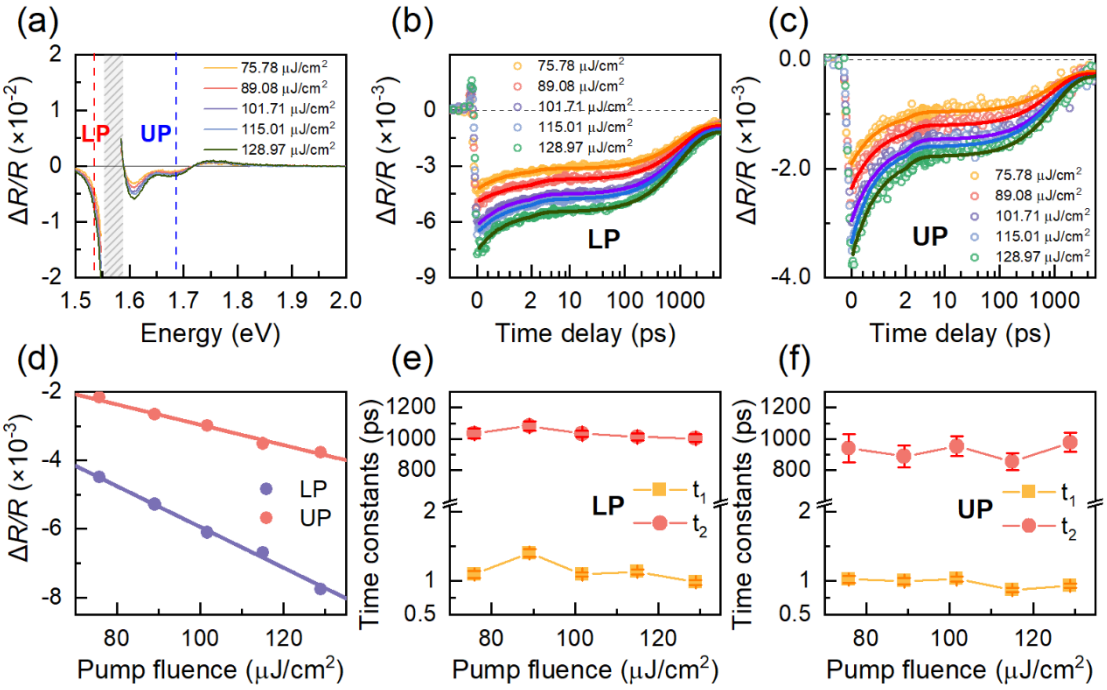

Supplementary Figure 13. Pump fluence dependent TR spectra of the 190 nm thick WSe_2 flake under 1.47 eV excitation. (a) Representative $\Delta R/R$ spectra at $T = 10$ ps. (b-c) Experimental dynamics (cycles) and fitted lines by a bi-exponential function of LP (b) and UP (c). (d) Minimum intensity at $T = 0$ fs of LP (violet) and UP (red) dynamics fitted by a linear function (lines), showing linear dependence with pump fluence. (e-f) Fitted time constants of LP (e) and UP (f) as a function of pump fluence.

Supplementary Table 2. Time constants of polariton dynamics of 170 nm thick WSe_2 flake under 1.47 eV excitation fitted by bi-exponential function.

Pump fluence	t_1^{LP}(ps)	t_2^{LP}(ps)	t_1^{UP}(ps)	t_2^{UP}(ps)
23.32	0.90±0.04	948.23±39.50	0.85±0.05	912.31±62.30
27.00	1.04±0.05	933.94±42.14	0.78±0.05	1045.08±83.36
30.68	1.00±0.04	1001.89±40.86	0.92±0.05	1054.55±68.24
34.36	0.91±0.03	904.57±29.60	0.91±0.04	908.67±47.33
38.04	0.93±0.04	905.86±36.15	0.97±0.04	930.29±45.85

Supplementary Table 3. Time constants of polariton dynamics of 190 nm thick WSe_2 flake under 1.47 eV excitation fitted by bi-exponential function.

Pump fluence (μJ/cm^2)	t_1^{LP}(ps)	t_2^{LP}(ps)	t_1^{UP}(ps)	t_2^{UP}(ps)
75.78	1.09±0.05	1034.74±33.45	1.02±0.05	939.86±89.56
89.08	1.40±0.06	1082.54±29.16	0.99±0.05	887.92±70.87
101.71	1.09±0.03	1032.30±20.84	1.02±0.04	951.84±63.38
115.00	1.13±0.04	1012.90±21.70	0.86±0.03	854.32±55.78
128.97	0.97±0.04	1004.03±24.57	0.92±0.03	976.82±60.86

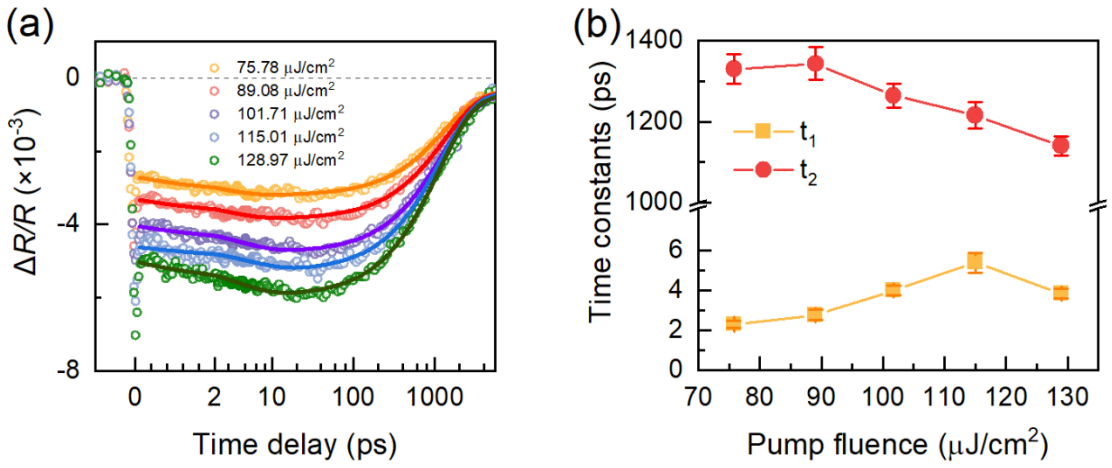

Supplementary Figure 14. Pump fluence dependent dynamics of ER peak of the 190 nm thick flake under 1.47 eV excitation. (a) Experimental dynamics (circles) and fitted curves by a bi-exponential function (lines) under different pump fluences. (b) Fitted time constants as a function of pump fluence.

As shown in Supplementary Fig. 14a, ER dynamics of the 190 nm thick WSe_2 flake (circles) under 1.47 eV excitation are fitted by a bi-exponential model (line), where t_1 represents the slow rise process and t_2 corresponds to the recombination process. The fitted parameters are listed in Supplementary Table 4. We observed that t_1 increases with increasing pump fluence. If the rise process is governed by PPA from LP, t_1 would be expected to decrease as the pump fluence increases, which contrasts with our experimental observations. This indicates that this slow rise is dominated by phonon assisted scattering. The increase of t_1 can be explained by the effect of phonon bottleneck, which usually limits fast polariton relaxation.[6] Similarly, it hinders the population transfer to ER due to the limited number of phonons.[6, 7] t_2 decreases with increasing pump fluence, indicative of an EEA dominated process.

Supplementary Table 4. Time constants of ER dynamics of the 190 nm thick WSe_2 flake under 1.47 eV excitation fitted by a bi-exponential function.

Pump fluence ($\mu J/cm^2$)	t_1(ps)	t_2(ps)
75.78	2.31±0.18	1330.06±35.88
89.08	2.77±0.26	1343.54±40.32
101.71	4.00±0.25	1264.66±29.23
115.00	5.39±0.50	1215.68±32.03
128.97	3.85±0.24	1140.85±23.91

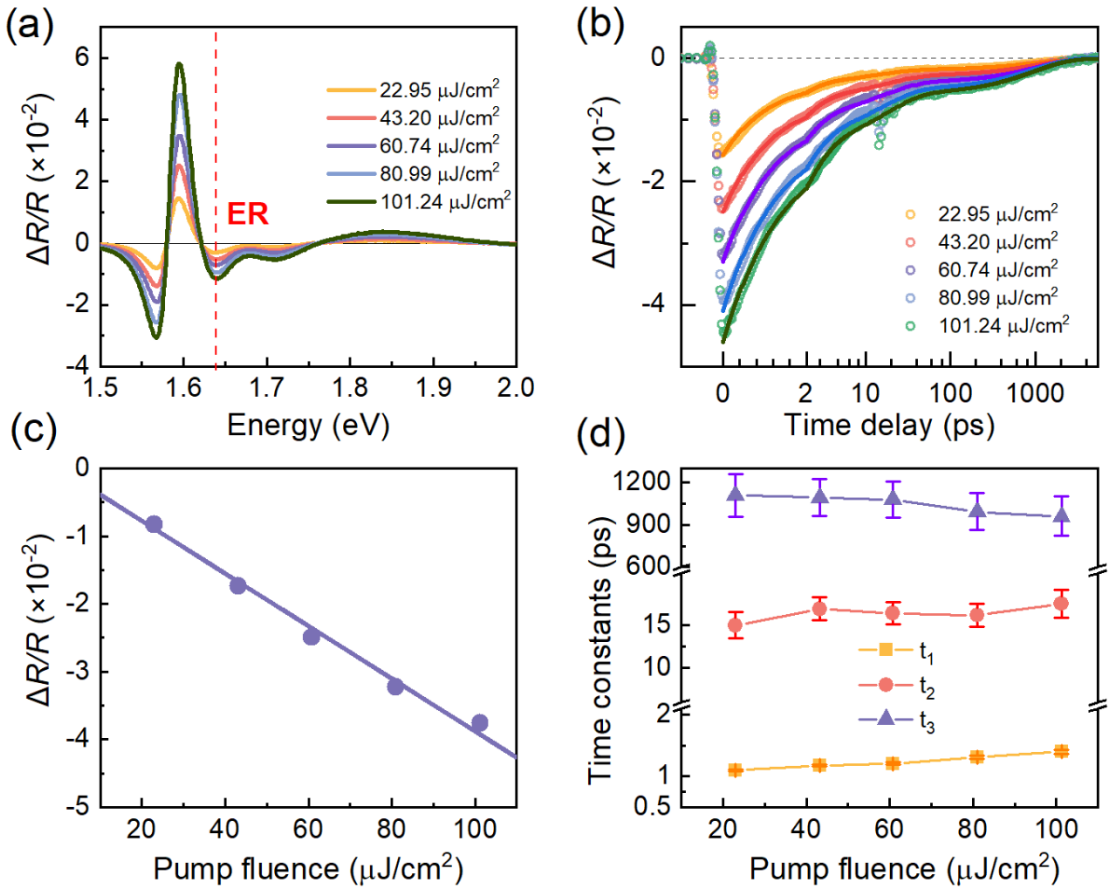

220

221 **Supplementary Figure 15. Pump fluence dependent TR spectra of the 170 nm**
222 **thick WSe_2 flake under 2.76 eV excitation.** (a) Representative $\Delta R/R$ spectra at $T = 10$
223 ps. (b) Experimental dynamics (cycles) and fitted lines by a bi-exponential function of
224 ER. (c) Minimum intensity at $T = 0$ fs of ER dynamics (symbols) fitted by a linear
225 function (lines), showing linear dependence with pump fluence. (d) Fitted time
226 constants of ER as a function of pump fluence.

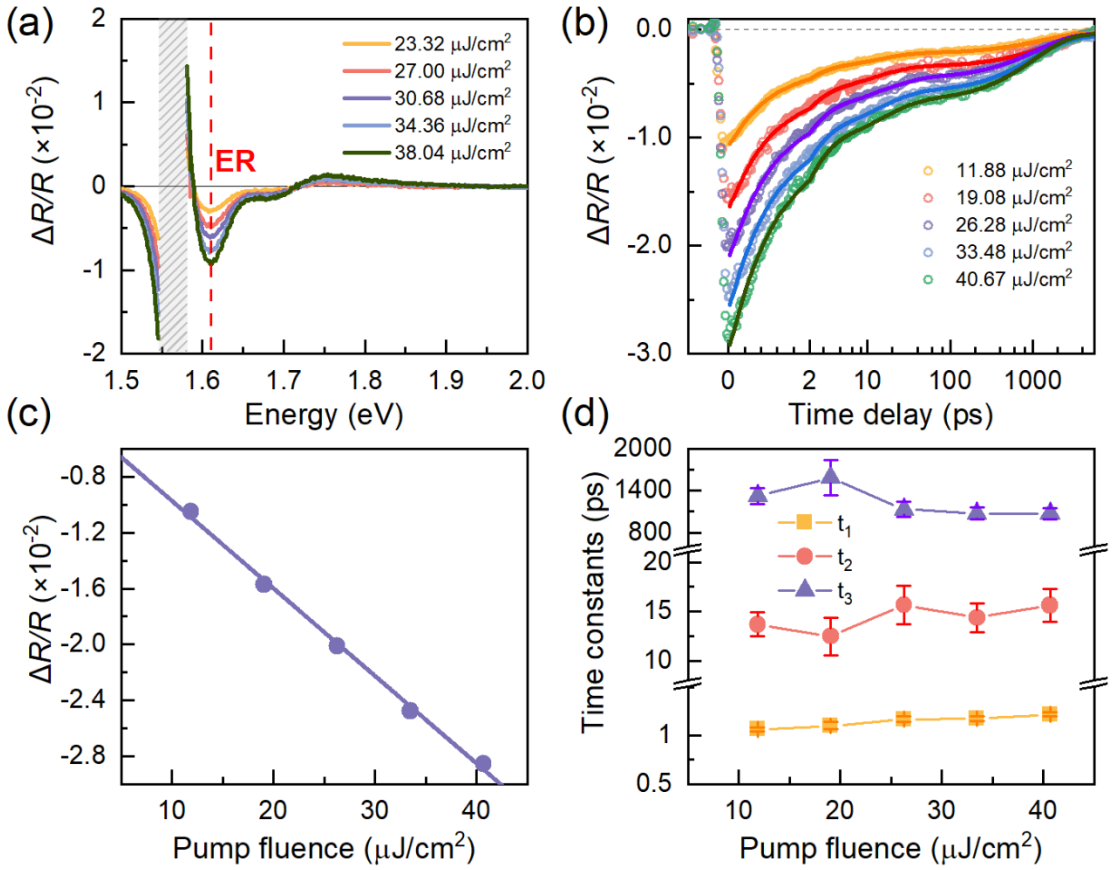

227

228 **Supplementary Figure 16. Pump fluence dependent TR spectra of the 190 nm**
229 **thick WSe_2 flake under 2.76 eV excitation.** (a) Representative $\Delta R/R$ spectra at $T = 10$
230 ps. (b) Experimental dynamics (cycles) and fitted lines by a bi-exponential function of
231 ER. (c) Minimum intensity at $T = 0$ fs of ER dynamics (symbols) fitted by a linear
232 function (lines), showing linear dependence with pump fluence. (d) Fitted time
233 constants of ER as a function of pump fluence.

234 We analyze the ER dynamics of 170 nm thick WSe_2 flake under 2.76 eV excitation
235 using a tri-exponential fitting (Supplementary Fig. 15b). The signal amplitudes of ER
236 show linear dependence with pump fluence (Supplementary Fig. 15c), confirming that
237 all experiments were carried out within the linear response regime of the sample. The
238 fitted time parameters are listed in Supplementary Table 5 and plotted in Supplementary

Fig. 15d. t_1 stands for the fastest relaxation process: exciton formation, and t_3 corresponds to the EEA dominated recombination process, respectively. We note that the relaxation dynamics of the bare AX in thinner, non-polariton flakes are not a tri-exponential process as observed in the strongly coupled samples. The emergence of the new fitting parameter t_2 in the latter indicates the presence of an additional relaxation channel. As shown in Supplementary Fig. 15d, t_2 remains essentially unchanged as the pump fluence increases. This indicates that this new relaxation channel is not strongly correlated with the photoexcited exciton density, and further suggests that the exciton-exciton scattering effect may not dominate the scattering process from the ER to the LP.

The results for the 190 nm thick flake are shown in Supplementary Fig. 16 and Supplementary Table 6, showing similar trends as that of the 170 nm thick flake.

Supplementary Table 5. Time constants of ER dynamics of 170 nm thick WSe_2 flake under 2.76 eV excitation fitted by tri-exponential function.

Pump fluence (μJ/cm^2)	t_1(ps)	t_2(ps)	t_3(ps)
22.95	1.10±0.02	14.93±1.50	1107.66±153.01
43.20	1.18±0.02	16.82±1.34	1092.01±130.40
60.74	1.21±0.02	16.35±1.25	1078.72±130.44
80.99	1.31±0.02	16.09±1.33	992.35±131.34
101.24	1.40±0.03	17.44±1.61	959.92±138.91

Supplementary Table 6. Time constants of ER dynamics of 190 nm thick WSe_2 flake under 2.76 eV excitation fitted by tri-exponential function.

Pump fluence (μJ/cm^2)	t_1(ps)	t_2(ps)	t_3(ps)
11.88	1.07±0.02	13.69±1.21	1322.58±111.86
19.08	1.10±0.04	12.48±1.90	1586.77±249.45
26.28	1.17±0.03	15.65±1.93	1133.21±109.20
33.48	1.17±0.03	14.37±1.49	1074.60±86.89
40.68	1.22±0.02	15.62±1.66	1066.71±79.46

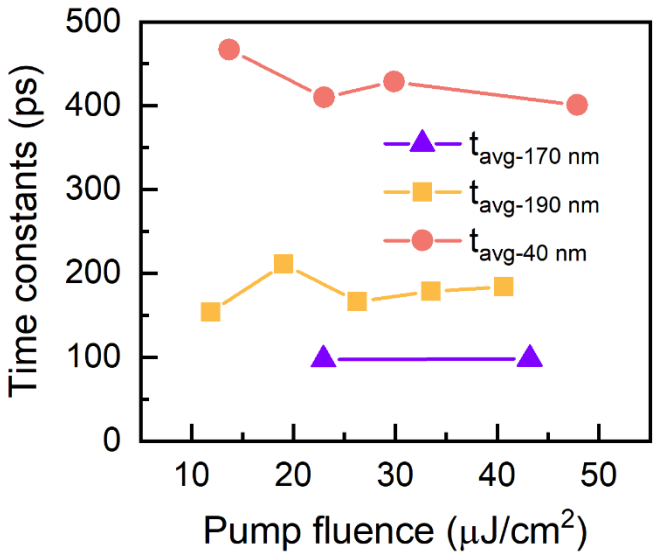

Supplementary Figure 17. **Average lifetime of ER of the 190 nm thick flake and AX of the 40 nm thick flake under 2.76 eV excitation.** t_{avg}^{40} is more than two times larger than t_{avg}^{170} and t_{avg}^{190} under similar excitation pump fluence.

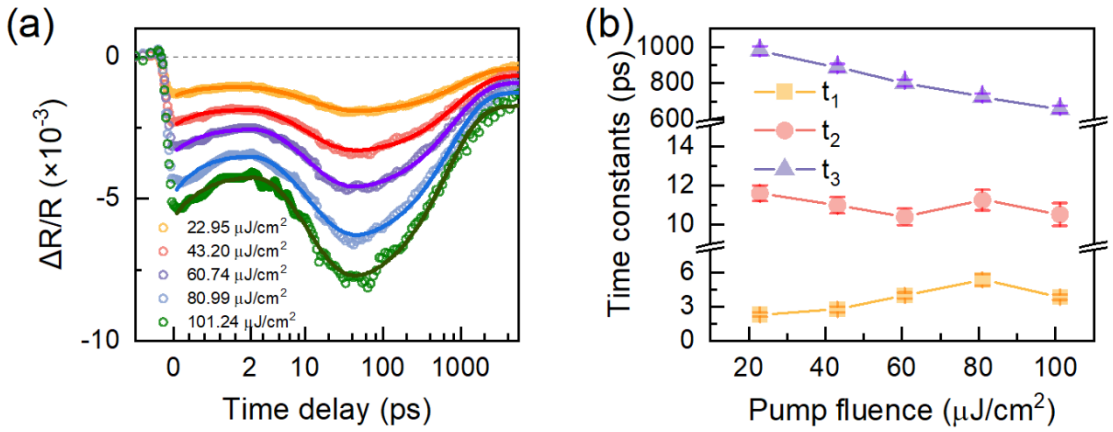

Supplementary Figure 18. Pump fluence dependent dynamics of LP of 170 nm thick flake under 2.76 eV excitation. (a) Experimental dynamics (cycles) and fitted lines by a tri-exponential function (lines) under different pump fluence. (b) Fitted time constants as a function of pump fluence.

We analyze the LP dynamics of 170 nm thick WSe_2 flake under 2.76 eV excitation using a tri-exponential fitting (Supplementary Fig. 18a). The fitted time parameters are listed in Supplementary Table 7 and plotted in Supplementary Fig. 18b. t_1 is the intraband relaxation process from high momentum state to the $k_{\parallel} = 0$ state. t_2 represents for the scattering process from ER to LP and shows no obvious pump fluence dependences. This observation further indicates that the exciton-exciton scattering effect may not dominate the scattering process from the ER to the LP. t_3 decreases with increasing pump fluence, originating from the gradual enhancement of exciton-polariton interactions.

Supplementary Table 7. Time constants of LP dynamics of 170 nm thick WSe_2 flake under 2.76 eV excitation fitted by tri-exponential function.

Pump fluence (μJ/cm^2)	t_1(ps)	t_2(ps)	t_3(ps)
22.95	2.31±0.18	11.62±0.40	979.64±24.41
43.20	2.77±0.26	11.01±0.42	885.98±22.04
60.74	4.00±0.25	10.41±0.42	802.18±18.86
80.99	5.39±0.50	11.27±0.53	724.22±20.61
101.24	3.85±0.23	10.54±0.58	656.55±20.37

Section 4. LP and UP dynamics at different probe energies.

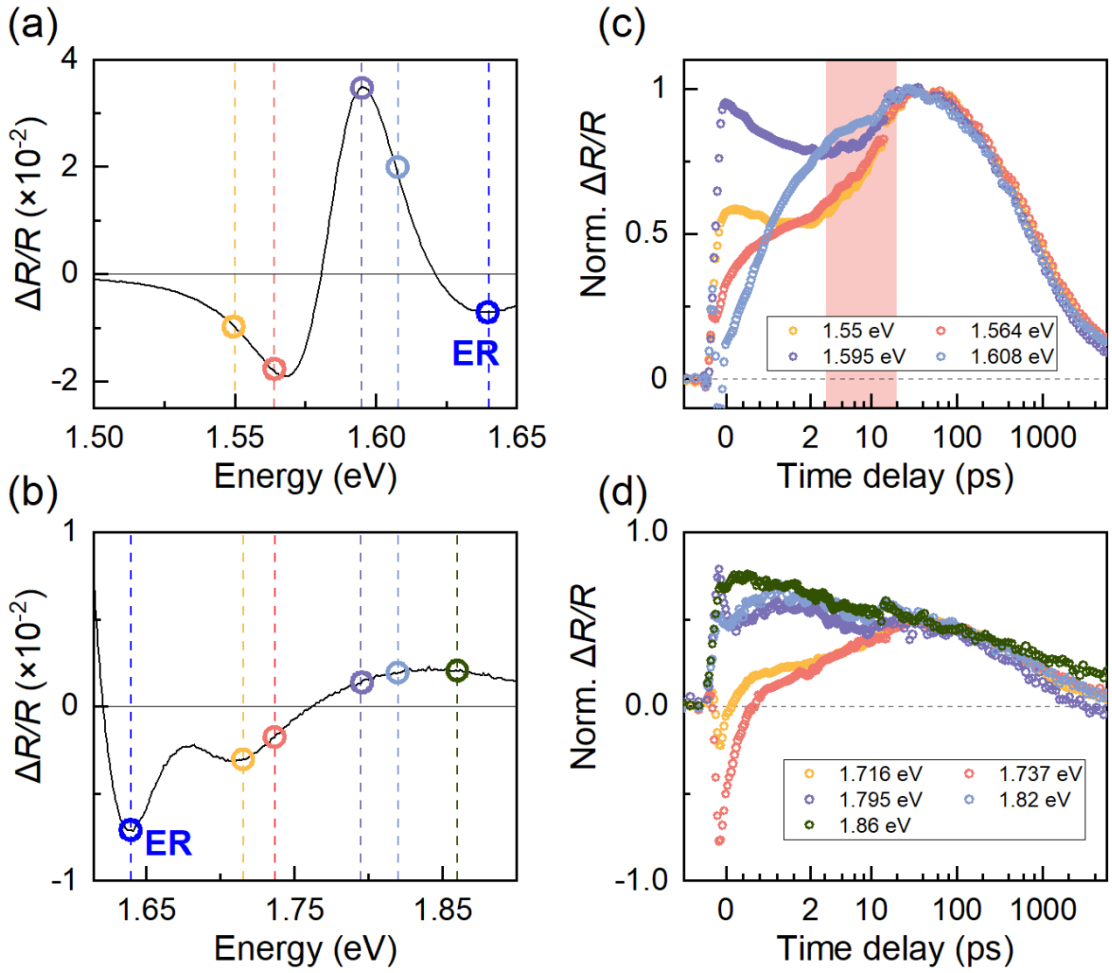

Supplementary Figure 19. LP and UP dynamics at different probe energies. (a,b) TR spectrum at $T = 10$ ps of the 170 nm thick WSe_2 flake under 2.76 eV excitation from 1.50 ~ 1.65 eV (a) and 1.60 ~ 1.90 eV (b). (c) LP dynamics at different energies corresponding to the circles and dashed lines in (a). (d) UP dynamics at different energies corresponding to the circles and dashed lines in (b).

We extracted and compared different LP dynamics at different energy positions, as shown in Supplementary Fig. 19a-b. A second rise process is observable at all traces. We observed that as the energy position approaches the ER peak, the extracted dynamics at 3~20 ps (red shaded in Supplementary Fig. 19c) become increasingly

influenced by the superposition effect of the ER, resulting in less pronounced rising dynamics before 10 ps. In contrast, when comparing the dynamics at different positions across the LP negative peak, significant differences are only observed within the initial 2 ps—where the LP and ER peaks shift most drastically. These suggest that the dynamics after 2 ps extracted from LP negative peak are suitable to present the intrinsic changes in the LP population.

As for UP dynamics, we found that the dynamics of the UP positive and negative peaks differ significantly, indicating that the UP positive peak is strongly modulated by the BX signal. However, the second rise process is also observable in the dynamics extracted from the negative signal. This suggests the presence of a scattering channel from the ER to the UP, occurring at the same time as that to LP.

Section 5. Raman spectra of the thick WSe_2 flakes.

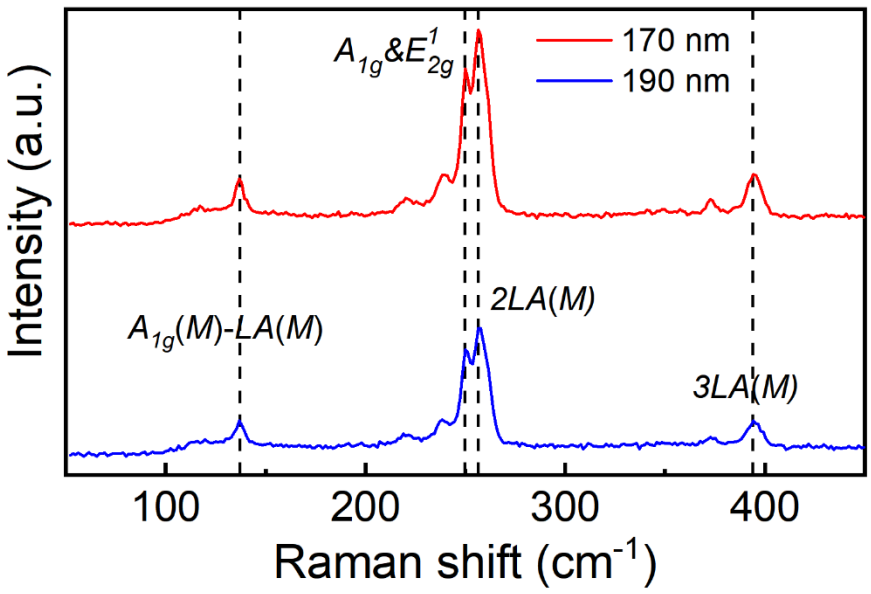

Supplementary Figure 20. Raman spectra of 170 nm (red) and 190 nm (blue) thick flake under 633 nm excitation.

To identify the phonon modes involved in the scattering processes, we measured the Raman spectra of the samples. In both samples, we observed four main Raman peaks at 137, 250, 256, and 394 cm^{-1}. Only the 250 cm^{-1} peak is attributed to the superposition of the optical phonon modes E^1_{2g} and A_{1g} (which are very close in frequency),[8] and others are all acoustic phonon modes ($A_{1g} - LA(M)$ at 137 cm^{-1}, $2LA(M)$ at 256 cm^{-1}, and $3LA(M)$ at 394 cm^{-1}).[8] Compared with monolayer WSe_2, the Raman intensities of optical phonon peaks in WSe_2 flakes are significantly reduced, while features associated with acoustic phonons become more pronounced.[8, 9] This suggests that scattering processes involving acoustic phonons play an important role in the electron–phonon interactions in our samples.

Section 6. Overlap of LP and ER peaks

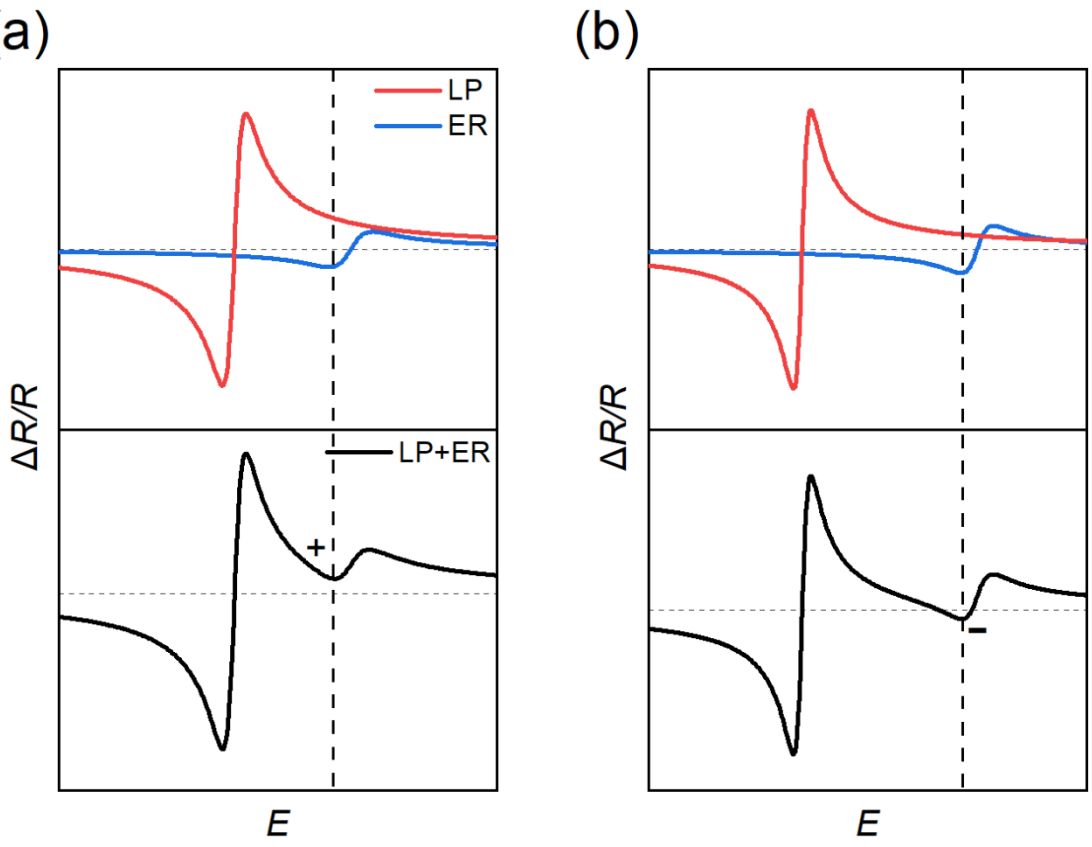

Supplementary Figure 21. Schematic diagrams of overlaps in blue detuned (a) and no detuning (b) flakes. The black dashed lines represent for the ER negative peak positions. ER negative peak become a positive dip in blue detuned simulation, but remain negative in no detuning one.

For the 170 nm thick flake, the positive dip (marked with red arrow in the zoom-in spectra in Fig. 3c) first emerges at 1.63 eV, decays rapidly within 2 ps, and then converts into a negative bleaching signal. In contrast, the response of ER of 190 nm thick flake at 1.61 eV is a negative signal at the beginning. We attribute this difference to the different exciton-cavity detuning and thus different spectral overlaps of the LP positive peak and the ER negative peak for the two flakes. For the 190 nm thick flake, the LP-ER energy difference is 97 meV, and thus there is no significant overlap.

Accordingly, ER appears negative after pump excitation and its dynamics exhibit a rapid rise and following a unique rapid decay process within the first 300 fs (blue line in Fig. 3g).

This makes the ER signal positive after pump excitation but still with a dip pointing to the negative (marked by red arrow in Fig. 3c inset). This also explains the weaker ER signal in the 170 nm thick flake compared to that of 190 nm thick flake. The initial dynamics at 1.63 eV (the ER negative peak position) is thus dominated by the strong, positive LP signal because it is resonantly excited. ER bleaching signal only becomes evident after the rapid relaxation of the LP signal.

Section 7. Polariton lifetime calculation

The lifetimes of UP (τ_{UP}) and LP (τ_{LP}) are determined by the weighted superposition of the lifetimes of cavity mode and exciton[10], that is,

$$\frac{1}{\tau_{UP}} = \frac{|\beta_{UP}|^2}{\tau_X} + \frac{|\alpha_{UP}|^2}{\tau_C} \quad (1)$$

$$\frac{1}{\tau_{LP}} = \frac{|\beta_{LP}|^2}{\tau_X} + \frac{|\alpha_{LP}|^2}{\tau_C} \quad (2)$$

where $|\alpha_{UP/LP}|^2$ and $|\beta_{UP/LP}|^2$ are the photon and exciton fraction in UP/LP, respectively (Fig. 2b and Supplementary Fig. 2b-c). τ_X is the exciton lifetime which is determined to be 750 ps by the ultrafast TR spectroscopic measurement (Supplementary Fig. 11). τ_C is the lifetime of the cavity mode of flakes, given by $\tau_C = \frac{\hbar}{\gamma_C}$, where $\hbar$ is the reduced Planck constant and γ_C is the half width at half maximum of the Lorentzian resonance of the calculated cavity mode in Supplementary Fig. 1. The parameters used for the calculations and the corresponding results are

presented in Supplementary Table 2. The results suggest that the polariton lifetime is dominantly determined by the short-lived cavity mode.

Supplementary Table 8. Parameters and results of polariton lifetime calculation.

Thickness (nm)	$\lvert\alpha_{LP}\rvert^2$	$\lvert\beta_{LP}\rvert^2$	$\lvert\alpha_{UP}\rvert^2$	$\lvert\beta_{UP}\rvert^2$	γ_C (meV)	τ_C (fs)	τ_X (ps)	τ_{LP} (fs)	τ_{UP} (fs)
170	0.17	0.83	0.83	0.17	71	9.3	750	54.4	11.1
190	0.52	0.48	0.48	0.52	76	8.7	750	16.7	18.0

References

1. Shen WD, Liu X, Huang BQ, Zhu Y, Gu PF. The effects of reflection phase shift on the optical properties of a micro-opto-electro-mechanical system Fabry-Perot tunable filter. *J. Opt. A: Pure Appl. Opt.* **6**, 853-858 (2004).

2. Golosovsky M, Neve-Oz Y, Davidov D, Frenkel A. Phase shift on reflection from metallodielectric photonic bandgap materials. *Phys. Rev. B* **70**, 115105 (2004).

3. Hazra S, Damari R, Golombek A, Flaxer E, Schwartz T, Fleischer S. Enhanced transmission at the zeroth-order mode of a terahertz Fabry-Perot cavity. *ACS Omega* **9**, 3000-3005 (2024).

4. Mirshafieyan SS, Luk TS, Guo JP. Zeroth order Fabry-Perot resonance enabled ultra-thin perfect light absorber using percolation aluminum and silicon nanofilms. *Opt. Mater. Express* **6**, 1032-1042 (2016).

5. Xiang B*, et al.* Two-dimensional infrared spectroscopy of vibrational polaritons. *P. Natl. Acad. Sci. USA.* **115**, 4845-4850 (2018).

6. Peng TY*, et al.* Polariton-mediated ultrafast nonlinear energy transfer in a van der Waals superlattice. *ACS Nano* **19**, 8152-8161 (2025).

7. Skolnick MS*, et al.* Polariton-polariton interactions and stimulated scattering in semiconductor microcavities. *Mater. Sci. Eng. C Biomim. Supramol. Syst.* **19**, 407-416 (2002).

8. Akintola K, Andrews GT, Curnoe SH, Koehler MR, Keppens V. Raman and Brillouin scattering studies of bulk 2H-WSe_2. *J. Phys. Condens.: Matter* **27**, 395401 (2015).

9. Blaga C, Alvarez AL, Balgarkashi A, Banerjee M, Morral AFI, Dimitrievska M. Unveiling the complex phonon nature and phonon cascades in 1L to 5L WSe_2 using multiwavelength excitation Raman scattering. *Nanoscale Adv.* **6**, 4591-4603 (2024).

10. Xu D*, et al.* Ultrafast Imaging of Polariton Propagation and Interactions. *Nat. Commun.* **14**, 3881 (2023).